Spreading and deposition of particulate matter in uniform flows

Étalement et déposition d'un matériau granulaire dans des écoulements uniformes

ANDREW J. HOGG, *Centre for Environmental and Geophysical Flows, School of Mathematics, University of Bristol, University Walk, Bristol BS8 1TW, U.K., email: A.J.Hogg@bristol.ac.uk*

HERBERT E. HUPPERT, *Institute of Theoretical Geophysics, Department of Applied Mathematics and Theoretical Physics, University of Cambridge, Silver Street, Cambridge CB3 9EW, U.K., email: heh1@esc.cam.ac.uk*

ABSTRACT
We consider the fate of a cloud of heavy particulate matter instantaneously released from either a line or a point source in a uniform ambient flow. The particles are advected by the flow as well as sedimenting from it. The behaviour of the current is determined by a non-dimensional parameter that represents the ratio of the advected flux of the ambient flow to the downward particle flux to the boundary. We determine the horizontal extent of the particulate matter and the density of the deposit as functions of time in terms of this parameter. In particular we evaluate the maximum upstream penetration distance of the particles. We also present the results of a series of experiments for a line release in a channel (the two-dimensional situation) and find excellent agreement between our theoretical predictions and the experimental data for: the upstream and downstream lengths of the current as functions of time; the final areal density of deposit on the floor; and the maximum upstream penetration of the current.

RÉSUMÉ
Nous examinons l'évolution d'un nuage de particules lourdes émis instantanément à partir d'une ligne ou d'un point source dans un écoulement uniforme. Les particules sont advectées par l'écoulement et parallèllement sédimentent. Le comportement du courant est déterminé par un paramètre adimensionnel qui représente le flux advectif rapporté au flux de particules sédimentant. Nous déterminons l'extension horizontale du nuage et la densité du dépôt à la paroi inférieure comme étant des fonctions de ce paramètre dépendant du temps. En particulier, nous évaluons la hauteur maximale d'ascension du nuage. Nous présentons également les résultats d'une série d'expériences effectuées dans le cas d'une ligne source émettant dans un canal (cas bi-dimensionnel). Nous trouvons un excellent accord entre les prédictions théoriques et les résultats expérimentaux en ce qui concerne : l'évolution temporelle et spatiale des longueurs caractéristiques du courant de particules, la densité surfacique du dépôt et la hauteur maximale de pénétration du nuage.

1. Introduction

Pollutant, introduced into a flowing stream, propagates some distance upstream. The mechanism of upstream penetration may be diffusion or, if the pollutant is of a different density to the stream, by buoyancy. The driving buoyancy interacts with advection effects and disperses the pollutant both downstream and upstream of its initial source point. Thus, for example, a sewerage outlet into a rapidly flowing river can have consequences for the water supply in a neighbouring town, even if the water is taken a considerable distance *upstream* of the sewage outlet point.

The aim of this paper is to present calculations of the propagation and dispersion of (heavy) particulate matter released into a uniform flow. To initiate some of the ideas, we first consider a source of fluid made heavy by the addition of a soluble component – a salt in water for example. We analyse both this situation and the more interesting situation of a particle-laden contaminant in both two-dimensional and axisymmetric geometries. These correspond to a line release in a channel and a point source release in a geometrically unconstrained fluid. We study the unsteady propagation of the cloud of dense fluid which arises from an instantaneous release. In this respect our analysis compliments and extends that of Alavian *et al.* (1992), who briefly discuss the steady intrusion of dense fluid into a co-flowing river.

In all situations the released fluid forms a gravity current (Simpson, 1997) which flows under a balance between buoyancy and inertial forces, if an appropriate Reynolds number is sufficiently high (as we shall assume), augmented by advection. Shortly after its initiation the current will become sufficiently long compared to its thickness that it is describable using the shallow water equations (Whitham 1974; Bonnecaze, Huppert and Lister 1993; Hallworth, Hogg and Huppert 1998; Huppert 1998). A slightly less rigorous, but much simpler, approach, which has the great advantage of leading to results which are describable analytically, is to develop a 'box model' for the current, wherein all horizontal variations at any particular time are ignored (Huppert and Simpson 1980; Dade and Huppert 1994). The results obtained in this way are generally in good agreement with those obtained from either numerical integration of the shallow water equations or from laboratory experiments (Hallworth, Hogg and Huppert 1998). It is this approach which we shall follow in this presentation.

The structure of the paper is as follows. Two-dimensional geometries are considered theoretically in the next section. Compositional currents are analysed first, in section 2.1, followed by particle-laden currents in section 2.2. The results of some laboratory simulations of these two situations are presented in section 3. Axisymmetric geometry, relevant to a point source release, is then considered in section 4. A summary, with conclusions and some practical applications, are presented in section 5.

2. Two-dimensional (line source) releases

2.1 Compositional currents

Consider the instantaneous release of a given volume V of fluid of density ρ_c into an ambient fluid of slightly lower density ρ_a (so that the Boussinesq approximation is valid) flowing with uniform velocity $\overline{U}$ in the (positive) x direction, as indicated in figure 1*. The resulting gravity current spreads along the (assumed) horizontal boundary at the base of the ambient fluid. Its motion is a consequence of the influences of gravity acting on the density and the advection of the mean flow. Consider the current at time t to extend distances $x(t)$ downstream and $y(t)$ upstream, as depicted in figure 1.

Assuming that entrainment of ambient fluid into the current can be neglected (Hallworth *et al.* 1993; 1996), we express the conservation of volume for the instanteously rectangular current of height h as

$$l \equiv x + y = A/h , \qquad (2.1)$$

where l is the total length of the current and A is the volume per unit width ($A=V/W$, where W is the width). The two extremities of the current propagate under the Froude number conditions (Benjamin 1968; Huppert and Simpson 1980)

$$\dot{x} = U + Fr(g'h)^{1/2} \quad \text{and} \quad \dot{y} = -U + Fr(g'h)^{1/2} , \qquad (2.2a, b)$$

where an overdot indicates a time derivative, the reduced gravity of the current $g' = (\rho_c - \rho_a)g/\rho_a$, U is the mean velocity in the x-direction experienced by the current and the Froude number $Fr=1.19$ (Huppert and Simpson 1980). Previous studies (Simpson and Britter 1980; Hallworth, Hogg and Huppert 1998) have suggested that $U = 0.6\,\overline{U}$ and this relationship is confirmed by the laboratory experiments reported in section 3.

Integrating (2.1) and (2.2), subject to the initial conditions that $x=y=0$ at $t=0$, we obtain

$$x = Ut + \gamma t^{2/3} \quad \text{and} \quad y = -Ut + \gamma t^{2/3} , \qquad (2.3a, b)$$

where

$$\gamma = \frac{1}{2}(3Fr)^{2/3}(g'A)^{1/3} , \qquad (2.4)$$

Differentiating (2.3b) and re-arranging the result indicates that the maximum upstream distance to which the current propagates, y_m, is given by $y_m = \frac{4}{27}\gamma^3/U^2 = \frac{1}{6}Fr^2 g'A/U^2$ and this distance is attained at the time $t_m = \frac{8}{27}(\gamma/U)^3 = \frac{1}{3}Fr^2 g'A/U^3$. Equation (2.3) indicates further that there is a time scale

$$\tau_c = (\gamma/U)^3 = \frac{9}{8}Fr^2 g'A/U^3 \qquad (2.5a, b)$$

at which the induced velocities due to buoyancy and the ambient flow are comparable. For times much less than τ_c the current evolves mainly due to buoyancy forces, and the effects of the mean flow in the ambient are much less significant. Alternatively, for times very much larger than τ_c effects due to the flow in the ambient dominate those due to buoyancy.

The overall length of the current

$$l \equiv x + y = 2\gamma t^{2/3} , \qquad (2.6a, b)$$

while twice the displacement of the centroid from its initial position

$$z \equiv x - y = 2Ut . \qquad (2.7a, b)$$

With the introduction of the lengthscale

$$l_c = \gamma^3/U^2 \qquad (2.8)$$

and the non-dimensional variables

$$L_c = l/l_c , \quad Z_c = z/l_c \quad \text{and} \quad T_c = t/\tau_c , \qquad (2.9a, b, c)$$

the relationships (2.6) and (2.7) become

$$L_c = 2T_c^{2/3} \quad \text{and} \quad Z_c = 2T_c , \qquad (2.10a, b)$$
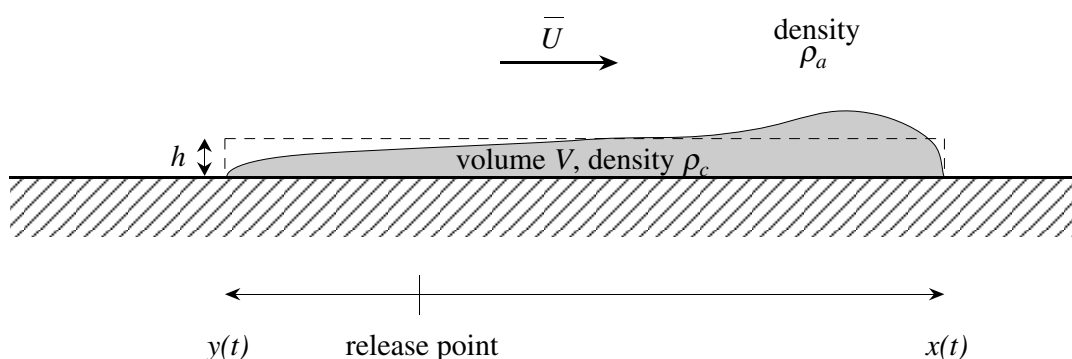
Fig. 1 Sketch of the gravity current with the box model representation dashed

which shows clearly that the length of the current increases as the two-thirds power of time while the centre of the current is swept downstream at a uniform velocity.

---

* We plan to present the results due to a continuous release in a subsequent publication.

Except for the premultiplicative constants, most of the above results can be obtained by dimensional analysis (Huppert 1997).

2.2 Particle-driven currents

The analysis of a monodisperse particle-laden current follows along similar lines. The major physical difference is that due to the gradual sedimentation of the particles from the flow to the underlying boundary, the density of the intruding current is progressively reduced. Mathematically, this is reflected in the Froude number conditions, which are expressed as

$$\dot{x} = U + Fr(g'_p \phi\, h)^{1/2} \text{ and } \dot{y} = -U + Fr(g'_p \phi\, h)^{1/2}, \quad (2.11a, b)$$

where $g'_p = (\rho_p - \rho_a)g/\rho_a$ is the reduced gravity of the particulate phase of density ρ_p and ϕ is its volume fraction. On the assumption that particles fall out of the flow at constant velocity V_s, and are not then re-entrained (Martin and Nokes 1988; Bonnecaze, Huppert and Lister 1993), the conservation of particles in the flow is expressed as

$$A\dot{\phi} = -V_s \phi\, l. \quad (2.12)$$

Expressions for x, y and ϕ, all as functions of t, can now be easily obtained by integrating (2.11) and (2.12), along with the conservation of volume relationship (2.1), subject to the initial conditions $x=y=0$ and $\phi=\phi_0$. Greater generality is obtained by first defining relevant length and time scales

$$l_\infty = [10 Fr(g'_p \phi_0 A^3)^{1/2}/V_s]^{2/5} \text{ and } \tau_\infty = 5A/(l_\infty V_s), \quad (2.13a, b)$$

and then using these to define L, $\overline{Z}$ and T as nondimensional values for length, twice the displacement of the centroid and time. In this way we obtain the expressions

$$\phi/\phi_0 = (1 - L^{5/2})^2,$$
$$T = \int_0^L \frac{s^{1/2}}{1 - s^{5/2}} ds \equiv F(L) \text{ and } \overline{Z} = \Lambda T \quad (2.14a, b, c)$$

in terms of the one non-dimensional parameter

$$\Lambda = 10UA/(l_\infty^2 V_s). \quad (2.15)$$

The relationships (2.14a,b) are graphed in figure 2.

As seen from (2.14) the current ceases ($\phi=0$) when $l=l_\infty$ ($L=1$), a value that is at first sight surprisingly independent of the ambient flow speed , although we note from (2.14b) that this length takes an infinite time to achieve (at least theoretically). The single parameter Λ reflects the influence of the mean flow on the runout of the gravity current and is proportional to the ratio of the mean flow to the settling velocity of the particle. Explicitly, expressing A as the product of the final runout length l_∞ and h_∞, the height of the current when this length is obtained, i.e. $A=h_\infty l_\infty$, we see that the value of Λ reflects the ratio of the horizontal flux of fluid, Uh_∞, to the vertical settling flux of particles, $V_s l_\infty$. When the flux of the mean flow is considerably larger than the particle settling
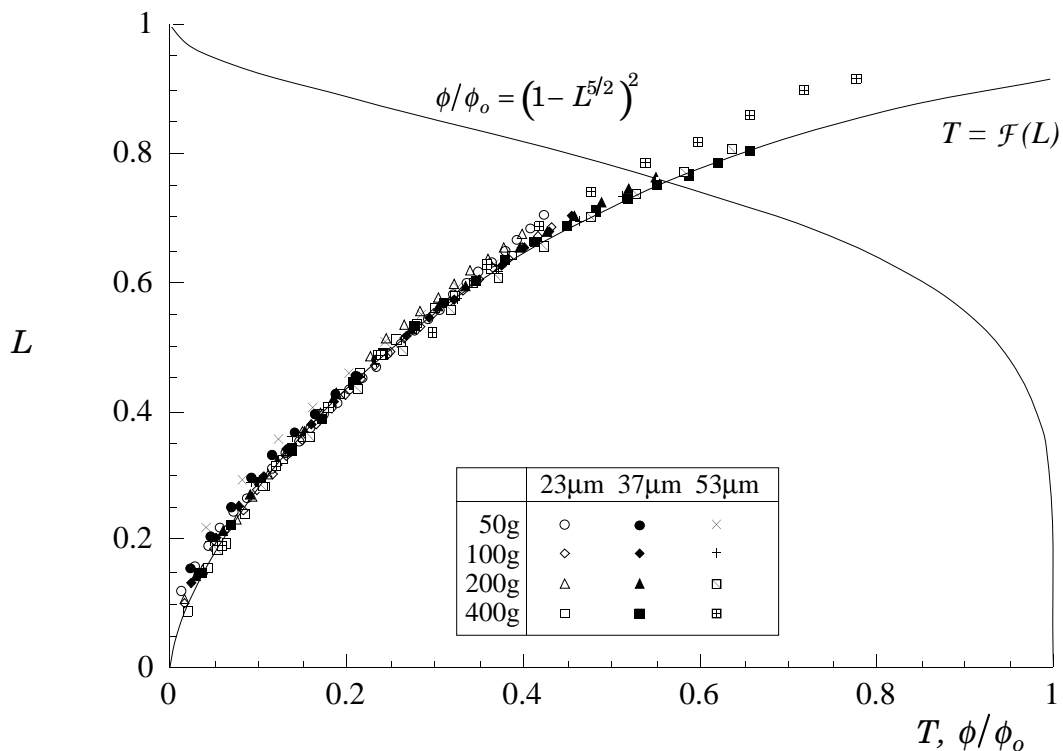
Fig 2. Non-dimensional length L plotted against non-dimensional time T, and non-dimensional particle concentration ϕ/ϕ_0. The solid curves are the theoretical relationships (2.14a,b). The symbols are experimental data for particle-laden currents with various masses and sizes of particles, as given in the legend, initially suspended in 2 litres of water before being rapidly released into the ambient flow.

flux (and thus $\Lambda >> 1$), the current is greatly influenced by the flow in the ambient. Alternatively, when $\Lambda << 1$, the propagation of the gravity current is relatively independent of the ambient flow.

The final spatial distribution of the deposit resulting from these particle-laden gravity currents may be calculated from the preceding box model analysis on assuming that the particles sediment out of the current uniformly along its length. When there is no flow in the ambient, the gravity current propagates symmetrically in the upstream and downstream directions, attaining its maximum length l_∞. In contrast, where there is a flow in the ambient, the centroid of the current is advected downstream, as indicated by (2.14c). The resulting deposit density is thus asymmetrically distributed about the initiation line of the two-dimensional current and extends a large distance downstream (and a smaller distance upstream). The final deposit density, $\eta(x)$, measured as a mass per unit area, can be evaluated from the integrated mass flux per unit area that is delivered to the bottom boundary while the current is overhead, which indicates that

$$\eta(x) = \rho_p V_s \int_{t_s}^{t_f} \phi \, dt \,, \tag{2.16}$$

where the limits of the integral correspond to the times at which deposition starts, t_s and finishes, t_f. Note that deposition commences when one of the fronts first passes overhead and continues until the rear of the current sweeps by. Substituting (2.14a,b) into (2.16), we find that

$$\eta(x) = \left(5\rho_p\phi_0 A \big/ l_\infty\right)\left[\tfrac{2}{3} L^{3/2} - \tfrac{1}{4} L^4\right]_{L_s}^{L_f}, \tag{2.17}$$

where L_s and L_f are the values of the non-dimensional length L at

the non-dimensional times T_s and T_f that correspond to the dimensional times t_s and t_f.

We present some illustrative graphs of $\eta(x)$ for different values of Λ in figure 3. Note that, as discussed above, when there is no flow in the ambient, i.e. when $U=\Lambda=0$, $\eta(x)$ is symmetric about the release line. As Λ increases, however, $\eta(x)$ becomes increasingly asymmetric.

Using our model, we can straightforwardly calculate numerically the maximum upstream distance to which the current propagates, d_+, as a function of Λ. The graph of $d_+(\Lambda)$ is presented in figure 4 and is well represented by the approximate, composite expansion (asymptotically correct in the two limits of very large or very small Λ) of

$$d_+ / l_\infty = \frac{\dfrac{1}{2} + \left(\dfrac{1}{5}\log\Lambda - \dfrac{\pi}{8}\right)\Lambda + \dfrac{1}{50}\Lambda^2}{1 + \dfrac{3}{25}\Lambda^4} \,. \tag{2.18}$$

3. Experiments

3.1 Experimental arrangements

To test the validity of our results and to evaluate the relationship between $\overline{U}$ and U, we conducted a series of experiments in a 9.4 m long Perspex channel, as sketched in figure 5. The channel has a rectangular cross-section 26 cm wide and 50 cm high and was filled with tap water to a depth H of 28.7 cm., A uniform ambient flow was established by pumping the water at a fixed rate in a continuous loop via a hose connecting inlet and outlet diffuser boxes situated at either end of the channel, thereby giving a working flow section of length 8.4 m. Each diffuser box comprised a
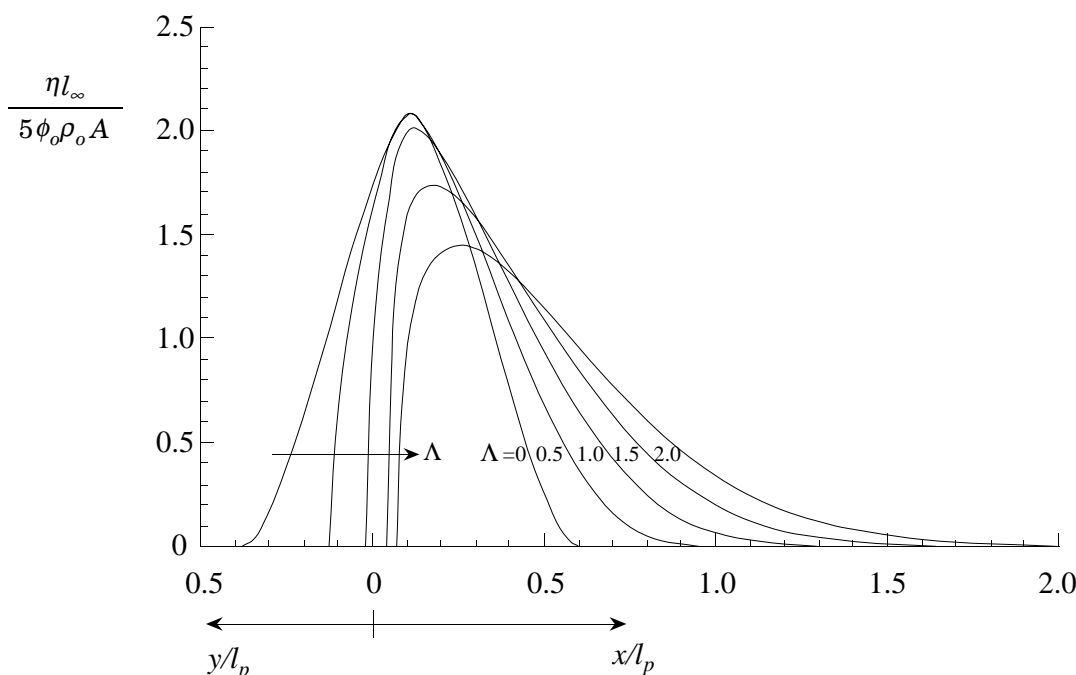
Fig. 3. Non-dimensional deposit thickness as a function of position for a range of values of $\Lambda = 10UA/(V_S l_\infty^2)$.
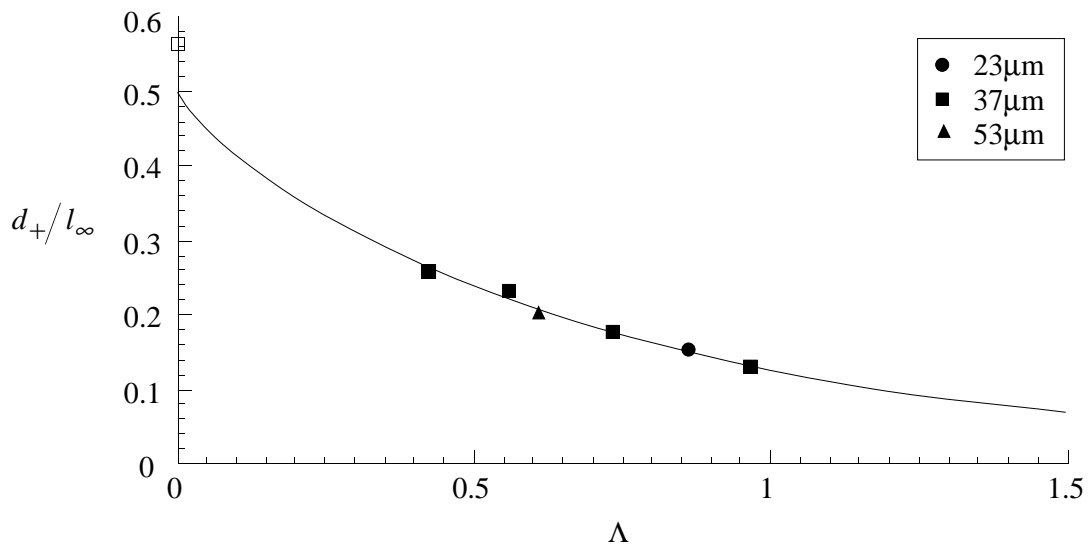
Fig. 4. The maximum non-dimensional upstream distance d_+/l_∞ as a function of $\Lambda = 10UA/(V_S l_\infty{}^2)$ given by (2.18). The symbols represent the results of experiments with different size particles, as indicated in the legend.
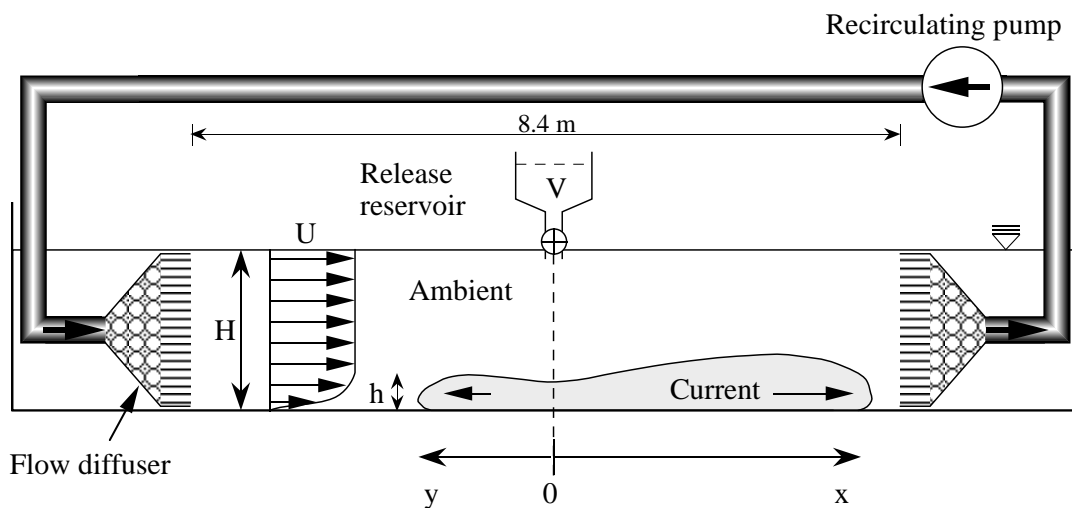
Fig. 5. Schematic diagram of the experimental apparatus (not to scale).

flared section packed with 1 cm diameter plastic balls and a horizontally aligned honeycomb section, designed to introduce and withdraw the flow evenly across the whole cross-sectional area of the channel. Profiles of the flow velocity as a function of depth were measured at several distances along the medial plane of the working section using a Sontek acoustic Doppler velocimeter (Lane *et al.* 1998). This non-intrusive device focuses an acoustic beam on a 0.5 cm^3 fluid sample volume and digitally translates the reflected signal into three mutually perpendicular velocity components, which we orientated to coincide with the major axes of the channel. Both the vertical and horizontal cross-stream velocity components were negligible. The horizontal downstream velocity components at various positions are presented as velocity profiles in figure 6. Each profile displays a fairly uniform velocity, $\overline{U}$, averaging 2.9 cm s^{-1} in the interior of the flow which reduces in value to zero at the channel floor through a lower boundary layer, approximately 2 cm thick. A reduction in flow velocity is also apparent as the free surface is approached. Integration of these flow profiles yielded an average volumetric flux of 1850

cm^{3}s^{-1}, which corresponds to a Reynolds number of approximately 7000.

The conventional lock-release method of instantaneously initiating a gravity current of fixed volume into a stationary ambient fluid was impossible to achieve in the present situation without severely disrupting the ambient flow. An alternative release mechanism was therefore designed whereby a fixed volume of dense fluid, initially held in a reservoir above the mid-point of the channel, was allowed to drain rapidly (in less than 1 s) into the flow stream through a 3 cm diameter tube positioned just beneath the free surface. The emergent jet of dense fluid inevitably entrained a significant volume of ambient fluid during its descent and subsequent lateral deflection upon impinging on the solid channel floor.

On testing our release mechanism in quiescent ambient conditions we found that the jet split equally and extended roughly 30 cm either side of the central release position before buoyancy forces, rather than momentum forces, began to dominate the motion. Entrainment of ambient fluid during this early phase was measured
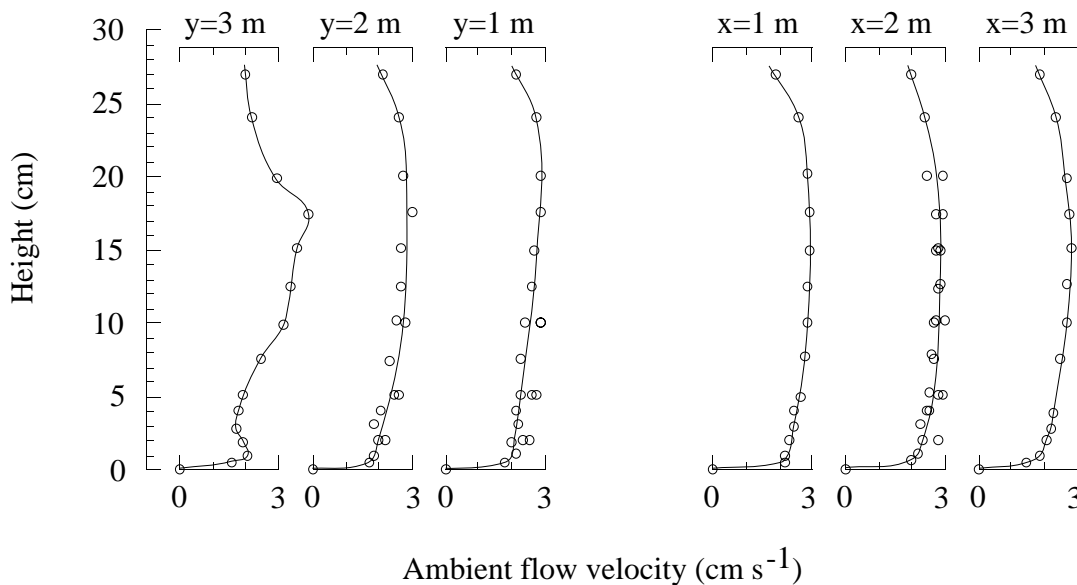
Fig. 6. Profiles of the horizontal downstream ambient fluid velocity as a function of depth, measured by acoustic Doppler velocimetry at various distances either side of the release position along the medial plane of the flow channel (in the absence of gravity currents). The structure in the profile at y = 3m is due to the proximity of this section to the input diffuser box.

to cause a dilution of the released fluid by a factor of approximately 20. This estimate was achieved by trapping a released current between vertical barriers which were positioned either 50 or 100 cm on either side of the entry point. When confined in this manner, the dense flow eventually settled to form a layer of constant composition. By measuring the height of this layer, its volume could be calculated and compared with the initial volulme. In each case our measurements indicated that the released fluid was diluted by a factor of 20 ±2 through entrainment of ambient fluid.

Buoyancy is conserved under mixing and so the initial dilution does not affect the value of the total buoyancy, $g'A$, in the calculation of the length and time scales for compositional currents [(2.5) and (2.8)]. For the particle-driven currents, however, the initial area occurs separately from the total buoyancy and so a knowledge of the initial dilution is vital for the scaling of these experimental results.

Measurements were made of the horizontal distance to the front of the current from the release point as functions of time in both the downstream (x) and upstream (y) directions by marking the position of the nose of the current at 3 second intervals. In the case of particle-driven gravity currents, the final distribution of sedimented particles was measured by recovering the mass of particles within a 5 cm wide strip across the width of the tank at various distances from the release point.

Compositional currents of different initial densities were generated by releasing 2 litres of water containing 50 g, 200 g and 400 g of dissolved salt into the ambient flow, resulting in initial values of g' of 17.1, 64.4 and 121 cm s^{-2} respectively. Solutions of each concentration were also released into a quiescent ambient for comparison. The currents released into a uniform ambient flow advanced both upstream and downstream, but were markedly asymmetrical. In the downstream (x) direction, the current was noticeably thicker than its counterpart in a static environment, and propagated with an increased velocity. As distance from the release point increased, the velocity of the current gradually decreased to a value approaching 0.6 times the mean ambient velocity. In the upstream (y) direction, the current was significantly retarded by the opposing ambient flow, and eventually came to rest. Prior to the final arrest, the current profile was observed to undergo a transition from the typical head and tail of a gravity current intruding quiescent surroundings into a much thinner wedge-shape within the lower boundary layer. Once in this form, dense fluid was continually stripped away from the upper surface of the arrested wedge by the action of interfacial eddies.

Figure 7 presents all the data we collected on the length and the position of the centroid of the current as functions of time. Also graphed in the figure are the two theoretical relationships (2.9). We see that there is very close agreement between theory and experiment for the length of the current and that the data for the position of the centroid indicates that U=0.6 $\overline{U}$, or that the centre of the current propagates downstream at a speed 0.6 times that of the ambient flow. This is in accord with an experimental result determined by Simpson and Britter (1980) using a considerably smaller experimental system.

3.2 Particle-driven currents

We generated numerous particle-driven gravity currents by releasing well-mixed suspensions of silicon carbide particles into water. The particles were fairly monodisperse, non-cohesive and had a density ρ_s= 3.217 g cm^{-3}. As a precaution, a small amount of Calgon was added to the suspension to prevent particle agglomeration. Three different particle sizes were used, with mean diameters of 23, 37 and 53 μm. Details of the size distribution with each grade are reported in Huppert *et al.* (1991). For each
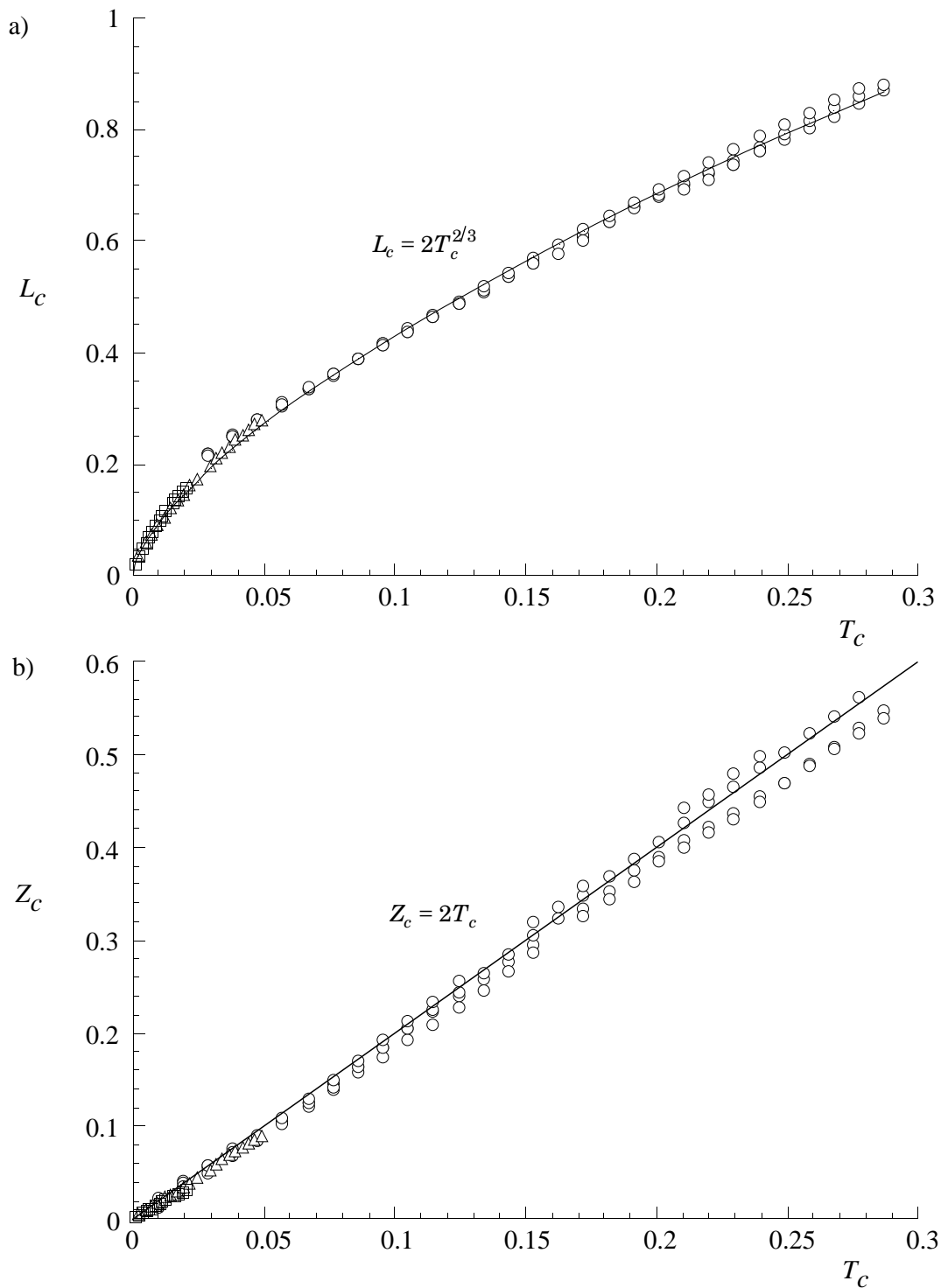
Fig. 7. a) Nondimensional length L_c, and b) nondimensional position of the centroid Z_c, plotted against nondimensional time T_c, all calculated assuming $U=0.6\ \overline{U}$, for composition alcurrents of 50g, ($\bigcirc$), 200g ($\triangle$) and 400g ($\square$) of salt dissolved in 2 litres of water, released into an ambient flow. The theoretical predictions (2.10) are included as solid lines in each graph.

particle size, experiments were run with four different initial particle masses of 50 g, 100 g, 200 g and 400 g suspended in 2 litres of water. Upon release, the particle-driven gravity currents propagated with decreasing velocity in both the x and y directions, while simultaneously depositing a sediment layer over the channel floor until all the particles had settled out, whereupon the current ceased to exist.

Velocities of the current at any point achieved by each flow were observed to increase monotonically with increasing initial mass of suspended sediment, and the current attained progressively longer maximum distances from the release point with decreasing particle diameter. The currents released into an ambient flow were markedly elongated in the downstream direction. The development of an arrested wedge of dense fluid in the upstream direc-
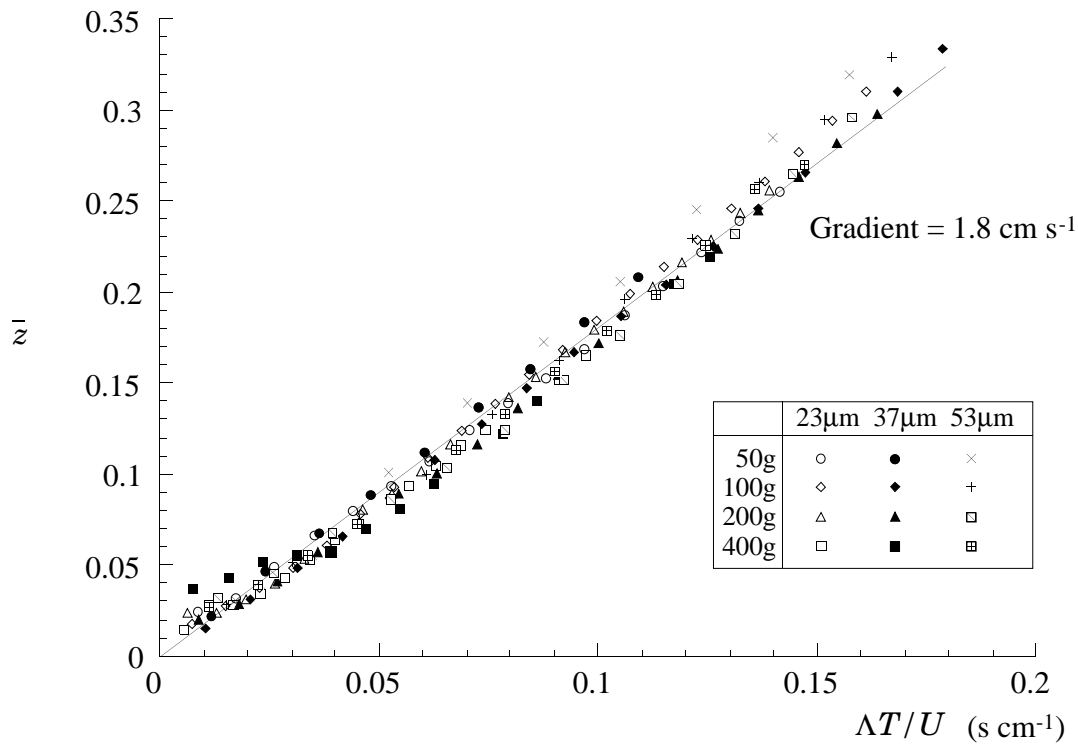
Fig. 8. Non-dimensional position of centroid $\bar{z}$, plotted against $\Lambda T/U$, for particle currents with various masses and sizes of particles (given by legend) initially suspended in 2 litres of water, released into an ambient flow. The solid curve is the best-fit straight line through all the data, the gradient of which determines U.

tion was not as noticeable as that seen in the compositional currents, since particles quickly sedimented from thinned flows in the slow moving lower boundary layer of the opposing stream.

We plot the non-dimensionalised experimental data in figures 2 and 8 along with the theoretical curves (2.14 b,c). We note that the non-dimensionalization collapses the experimental data and that there is very good agreement with the theoretical predictions. From the comparison shown in figure 8 we find that U=0.62 $\bar{U}$, in agreement with the result obtained from the compositional currents.

Once all the particles had settled out, the final length of the deposited layer was recorded, and its mass distribution measured by 'vacuuming up' the sediment using a siphon tube within a 5cm x 25 cm rectangular 'pastry cutter' placed over the layer at specific intervals. The mixture was collected in a beaker, the water decanted and the particles dried and weighed to determine the mass of deposit per unit area. As a check on the sampling method, the total mass of sediment was recovered by integrating the measured deposition profile. The value obtained in this way was generally found to be within 1% of the initial value. We compare some of the experimentally measured deposit profiles with the theoretical predictions for four values of Λ in figure 9. The agreement is seen to be very good and in particular the asymmetry predicted by the theory is accurately reflected by the data.

4. Axisymmetric currents

We now develop a theoretical model of the spreading of an intrusion of relatively dense fluid released from a point source within a uniform ambient flow. In the absence of an ambient flow, the dense fluid propagates radially away from its source. Its rate of propagation may be modelled using a box-model approach, which yields results in good agreement with experimental measurements for both compositional currents (Huppert & Simpson 1980) and particle-driven currents (Dade & Huppert 1995, Bonnecaze *et al.* 1995). In this section we extend the box-model analysis to incorporate the effect of a unidirectional flow. The spreading of dense fluid is no longer radial and we calculate the locus of points which corresponds to the front of the gravity current. The gravity current never reaches the area outside this locus.

Axisymmetric models of gravity currents may be equally well applied to flows within an angular sector, provided that the boundaries of the sector have only a negligible influence. (This is equivalent to requiring that the lengthscale associated with the gravity current be much larger than that of the boundary layer.) Hence this study may be applied to discharges of dense fluid at the boundary of a relatively wide channel flow, such as a river or an estuary.

In the following subsections we develop box models of gravity currents driven by either a compositional difference or the suspension of particles in the presence of a mean flow. Our emphasis is to establish the extent of the region within which the intrusion will propagate and, for particle-driven gravity currents, to calculate the distribution of the deposited sediment.

4.1 Compositional currents

We consider the instantaneous intrusion of a finite volume of
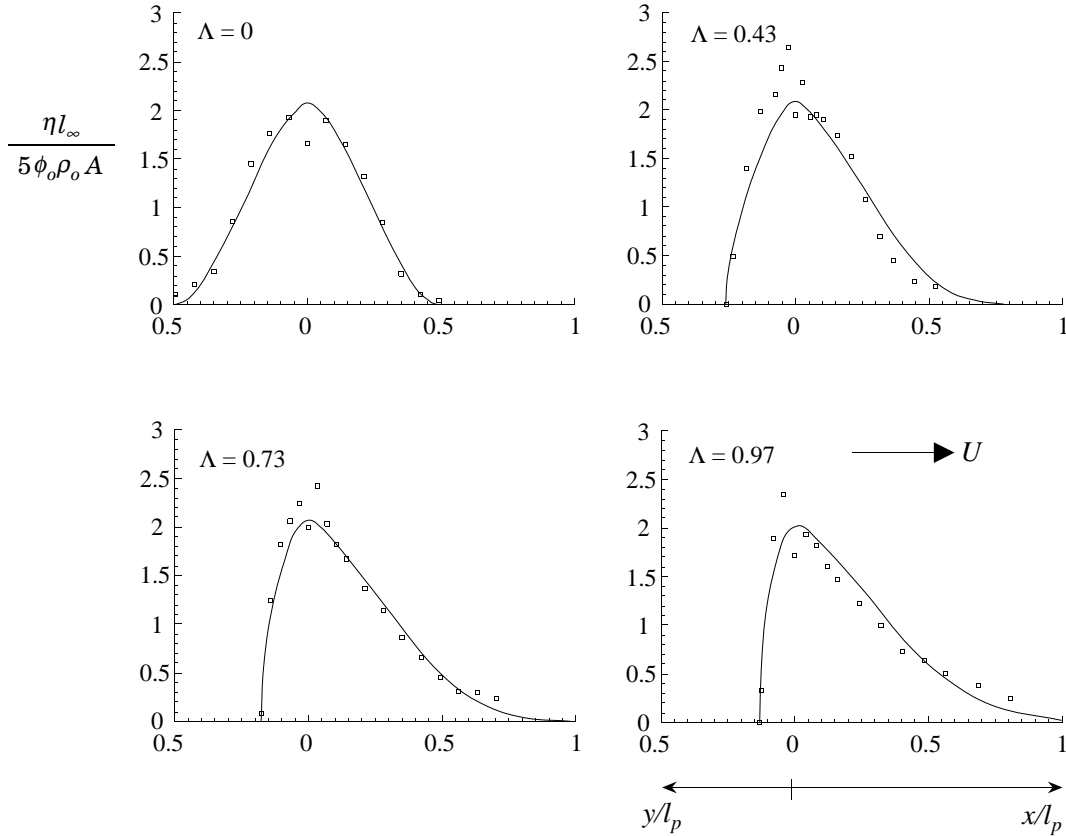
Fig. 9. Plots of the experimentally measured deposit profiles and the theoretical predictions for four different values of $\Lambda = 10UA/(V_S l_\infty^2)$.

fluid with a density ρ_c into an ambient fluid of lower density ρ_a. Driven by gravity, the intruding fluid spreads along the horizontal boundary underlying the ambient fluid, which flows uniformly in a horizontal direction. We define horizontal coordinate axes such that the x-axis is aligned with this uniform flow and the y-axis is perpendicular to the flow. As in §2.1, it is convenient to formulate the equations governing the evolution of the flow in a frame of reference which moves with the velocity of the centroid of the intrusion. In this frame the gravity current spreads radially in the form of a uniform disk whose radius and height change with time. Denoting the radial distance from the centroid by r, we may express the conservation of fluid volume of the current by

$$r^2 h = V , \qquad (4.1)$$

where h is the height of the current and V is twice the volume per unit (radian) angle. (The total volume is πV, which remains constant during the evolution of the current.) The rate of radial expansion of the gravity current in this moving frame is given by

$$\dot{r}(t) = Fr(g'h)^{1/2} , \qquad (4.2)$$

where, as before, $g' \equiv (\rho_c - \rho_a)g/\rho_a$ is the reduced gravity of the current and Fr is the frontal Froude number, which is assumed to be constant. Substitution of (4.1) into (4.2) and integration, subject to the initial condition that $r=0$ at $t=0$, yields

$$r = [2Fr(g'V)^{1/2}t]^{1/2} . \qquad (4.3)$$

Denoting the position of the centroid by $\bar{x}_b$ we write

$$\bar{x}_b = Ut , \qquad (4.4)$$

where U is the velocity experienced by the gravity current in response to the ambient flow. (Recall that for two-dimensional gravity currents it was established that U was 0.6 of the mean flow.) At this stage it is convenient to identify the time and length scales

$$t_a = 2Fr(g'V)^{1/2}/U^2 \text{ and } r_a = 2Fr(g'V)^{1/2}/U \qquad (4.5a, b)$$

which may be used to non-dimensionalise the relationships (4.3) and (4.4). The timescale t_a corresponds to the time at which the velocity of the gravity-driven motion and the uniform flow are comparable, while the lengthscale r_a is the downstream distance moved at this time. Writing the dimensionless variables as $R_a = r/r_a$, $\bar{X}_a = \bar{x}_b/r_a$ and $T_a = t/t_a$, and $T_a = t/t_a$, we find that

$$R_a = T_a^{1/2} \text{ and } \bar{X}_b = T_a . \qquad (4.6a, b)$$

Hence the boundary of the spreading gravity current, expressed in terms of a fixed frame of reference in which X_a and Y_a are dimensionless horizontal coordinates, is given (as a function of

time) by

$$(X_a - \overline{X}_b)^2 + Y_a{}^2 = R_a{}^2. \tag{4.7}$$

We may therefore determine the bounding region within which the current propagates. This is obtained by evaluating the maximum extent of the curves (4.7). Setting to zero the derivative with respect to T_a of (4.7), which occurs at time τ say, we determine the parametric form of this bounding curve to be given by

$$X = \tau - 1/2 \quad \text{and} \quad Y^2 = \tau - 1/4 \tag{4.8a, b}$$

in the horizontal, dimensionless co-ordinate system (X, Y). Hence, in these non-dimensional variables, the region is given by the parabola

$$Y^2 = X + 1/4 \tag{4.9}$$

4.2 Particle-driven currents

A conceptually similar model may be developed to describe the gravity-driven flow of a particle-laden intrusion within a uniformly flowing ambient. This motion, however, is complicated by the sedimentation of particles from the current to the lower boundary which progressively reduces the density, and hence the buoyancy-induced propagation velocity is also reduced. Box-model equations for the conservation of fluid volume and the rate of radial propagation may be formulated in a frame of reference moving with the centroid. They yield

$$r^2 h = V \tag{4.10}$$

and

$$\dot{r}(t) = Fr(g'_p \phi \, h)^{1/2} \tag{4.11}$$

Particle settling is modelled in an analogous manner to §2.2 to yield

$$V\dot{\phi} = -V_s \phi r^2 \tag{4.12}$$

Thus from (4.11) and (4.12) we find that

$$\left(\frac{\phi}{\phi_0}\right)^{1/2} = 1 - \frac{V_s r^4}{8Fr(g'_p \phi_0 \, V^3)^{1/2}} \,, \tag{4.13}$$

where ϕ_0 is the initial volume fraction of particles.
These relationships suggest the use of the length and time scales

$$r_p = \left[\frac{8Fr(g'_p \phi_0 V^3)^{1/2}}{V_s}\right]^{1/4} \quad \text{and} \quad t_p = \left[\frac{4V}{V_s r_p{}^2}\right] \tag{4.14a, b}$$

to non-dimensionalise the governing equations. The lengthscale r_p corresponds to the radius of the particle-driven intrusion at which the volume fraction vanishes. Defining the dimensionless

variables as $R_p = r/r_p$, $\overline{X}_p = \overline{X}/r_p$, $T_p = t/t_p$ and $\Phi = \phi/\phi_0$ and integrating the equations of motion, we obtain

$$R_p = \tanh^{1/2} T_p \tag{4.15a}$$

$$\Phi = \operatorname{sech}^4 T_p \tag{4.15b}$$

and

$$\overline{X}_p = \lambda T_p \,. \tag{4.15c}$$

In these expressions there remains a single dimensionless parameter,

$$\lambda = \frac{4UV}{r_p^3 V_s} \,, \tag{4.16}$$

which measures the magnitude of the horizontal flux of fluid against the vertical settling flux. (It is analogous to the parameter Λ introduced in §2.2.)

These equations govern the temporal evolution of the radius and volume fraction of particles of the particle-laden cloud in a frame moving with the centroid. In a fixed frame of reference, the perimeter of the cloud is given by

$$\left(X - \lambda T_p\right)^2 + Y^2 = R_p{}^2 \,. \tag{4.17}$$

The region within which the gravity current propagates can now be calculated by differentiation of (4.17) with respect to T_p (as before). The result corresponds to the boundary of the region within which particles are deposited from the current. The boundary of this region, in parametric form, is given by

$$X = -\frac{\operatorname{sech}^2 \tau}{2\lambda} + \lambda \tau \tag{4.18a}$$

and

$$Y = \left(\tanh \tau - \frac{\operatorname{sech}^4 \tau}{4\lambda^2}\right)^{1/2} \,. \tag{4.18b}$$

We plot these loci in figure 10. The maximum upstream distance, X_m, propagated by the current may be calculated numerically by finding the value of the parameter τ from (4.18b) for which $Y=0$ and then substituting this value into (4.18a). The distance X_m may be evaluated analytically in the regimes of weak ($\lambda \ll 1$) and strong ($\lambda \gg 1$) ambient flows relative to the initial buoyancy-induced speed of propagation. We find that

$$X_m = -1 + \tfrac{1}{2}\lambda\left(1 + \ln 2 - \ln \lambda\right) - \tfrac{1}{8}\lambda^2 + O(\lambda^4) \quad (\lambda \ll 1)$$

$$= -\frac{1}{4\lambda} + \frac{1}{192\lambda^5} + O\left(\frac{1}{\lambda^9}\right) \quad (\lambda \gg 1) \tag{4.19a, b}$$

which are plotted in figure 11.
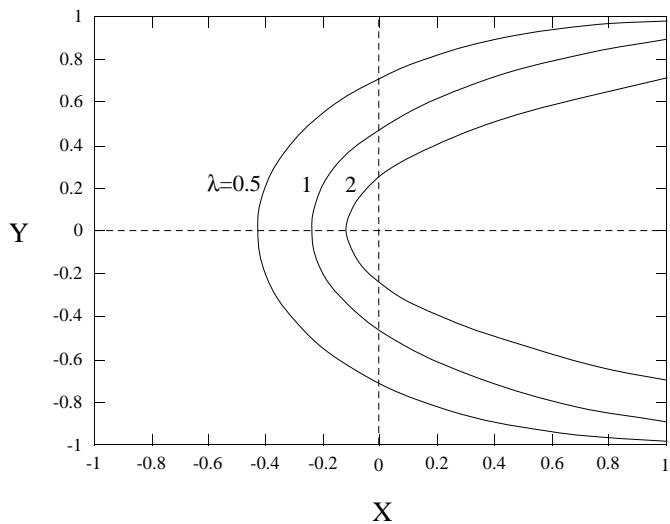
Fig. 10. The boundary of the region within which the particle-driven gravity current propagates for λ=0.5, 1, 2.

The distribution of the deposit arising from the flow of the particle-driven intrusion may be calculated in a manner analogous to §2.2. It is assumed that the particles sediment out of the flow uniformly throughout the area covered by the particle-laden cloud. Therefore at a dimensional location (x,y) the deposit measured in mass per unit area is given by

$$\eta(x, y) = t_p \rho_p V \phi_0 \int_{T_s}^{T_f} \Phi \, d\tau \qquad (4.20)$$

where T_s and T_f are the dimensionless times at which sedimentation starts and finishes at this particular location. If the dimensionless position, (X,Y), falls outside of the locus given by (4.18) there is no deposit. Conversely if the position lies within

the locus the deposit is given implicitly by

$$\eta(X, Y) = \left(4V\rho_p / r_p^2\right)\left[R_p^2 - \tfrac{1}{3} R_p^6\right]_{R_s}^{R_p} \qquad (4.21)$$

where the terms within the square bracket are evaluated at the upper and lower limits of R_f and R_s which are the dimensionless radii of the intrusion corresponding to the times T_f and T_s, respectively. In figure 12 we plot contours of the deposit, noting that the degree of asymmetry is a function of the parameter λ.

5. Conclusion

We have analysed the propagation, dispersion and deposition of a cloud of small, heavy particulate matter in a uniform horizontal ambient flow above a flat base. Results were obtained using a box-model approach, wherein the current was assumed to have properties that at any time did not vary in the horizontal direction. This approach allowed us to determine results in analytical form (rather than from the much more cumbersome numerical integration of a series of partial differential equations). We considered both line source (two dimensional) and point source (axisymmetric) instantaneous releases of the particles. Results obtained from careful experiments of the former situation were in good agreement with our theoretical predictions for the rate of propagation of the cloud of particles, and for the final distribution of the deposit at the base. The experiments also indicated that the effective velocity experienced by the spreading current is 60% of the total flow in the ambient.

Our results will be directly appropriate for a slowly varying ambient flow as long as the time-scale of the variation is significantly greater than the time-scale of the depositing flow, given in two dimensions, by τ_∞ in (2.13b) or, in the axisymmetric situation, by
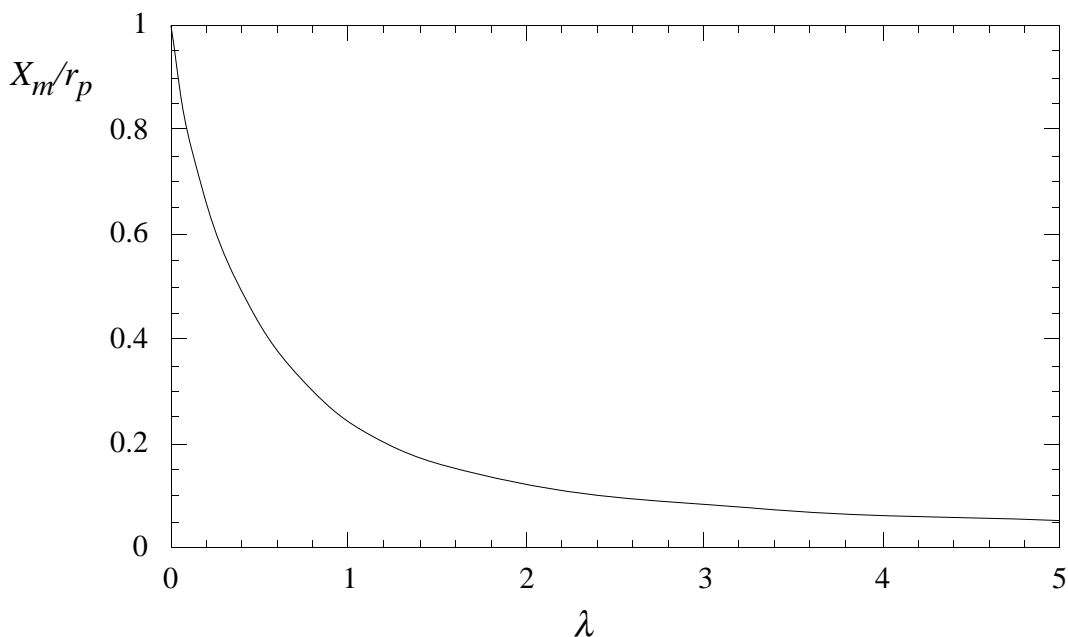
Fig. 11. The maximum non-dimensional upstream penetration distance X_m/r_p as a unction of $\lambda=4UV/(r_p^3 V_s)$ for the instantaneous release of a particle cloud from a point source in a unidirectional ambient flow.
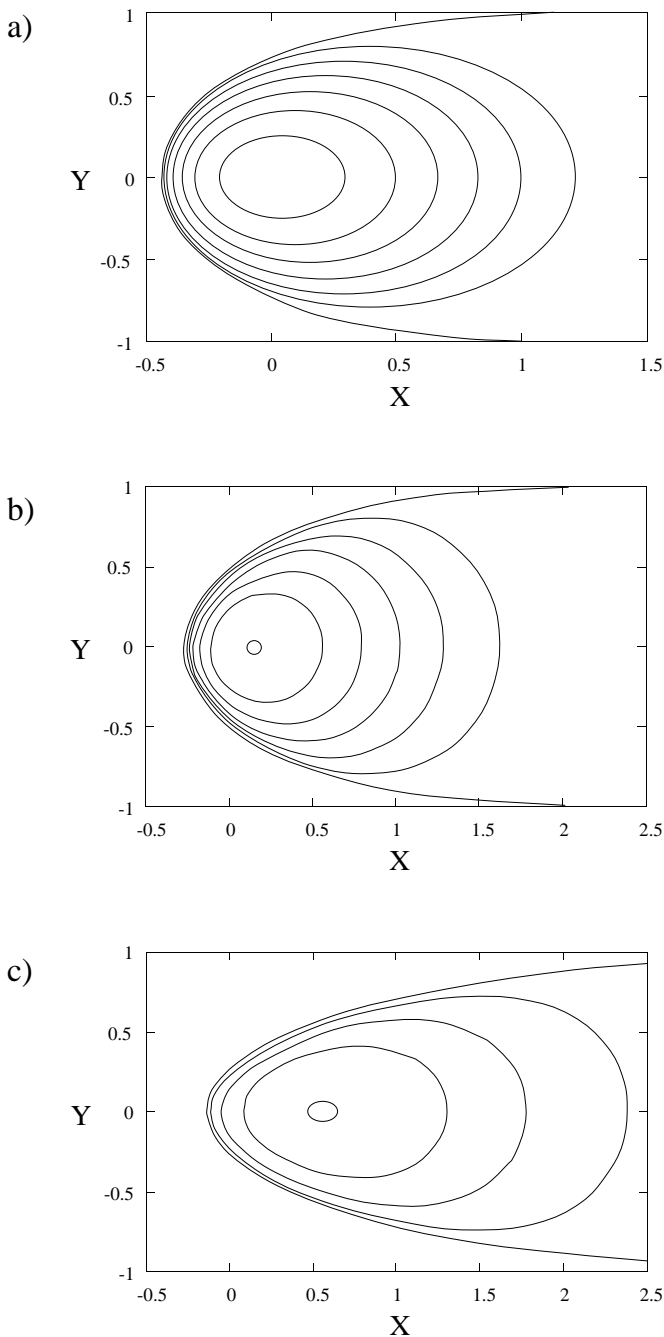
Fig. 12.   a) Contours of the distribution of the deposit per unit area. The deposit has been non-dimensionalised with respect to $4V\rho_p/r_p^2$ and a) $\lambda = 0.5$, b) $\lambda = 1$ and c) $\lambda = 2$, The contours are shown at intervals of 0.1 in the range 0-0.6 for a) and b), and 0-0.4 for c).

t_p in (4.14b). Alternatively, for more rapidly varying ambient flows, the governing equations we have proposed could be integrated numerically. From this integration the rate of propagation of the front and the resultant deposit could be obtained for an arbitrary flow. In addition, whilst our results were derived on the assumption of an instantaneous release they will carry over unaltered to a less rapid release as long as the release time is significantly less than either τ_∞ or t_p as appropriate.

In the two-dimensional situation the flow varies with the parameter $\Lambda=10UA/(l_\infty^2 V_s)$, as given by (2.15), which represents a ratio

of the horizontal advective flux of the ambient flow to the downward particle flux within the flow. The maximum upstream penetration is given (to a high degree of approximation) by (2.18). The particle concentration within the current as a function of time and position is given by (2.14) and the final deposition density by (2.17). In the alternative situation where the particle dispersion is axisymmetric, representing a horizontally unconfined geometry, the governing parameter is $\lambda=4UV/(r_p^3 V_s)$. The horizontal extent of the current is given by (4.18) with the final deposit density expressed by (4.21).

To obtain some quantitative feeling for our results, consider the following three examples. The first is relevant to the influence of a mean current or the tides on the dredging of sand from a harbour bed using the new technique of expelling a jet of water vertically onto the sea bed (Huppert 1998). The second is relevant to the cleansing of sewage in a settling tank (de Rooij 1999). The third has application to a severe dust storm in the atmosphere (Simpson 1997).

For the first example consider the particulate matter to be 20 μm in diameter and have an excess density of 1 g cm^{-3}, which implies a settling velocity in water of 0.022 cm s^{-1}. Consider the suspension of particles to have concentration 5% by volume and cross-section (in the two-dimensional situation) of 100 m^2, which indicates a length-scale l_∞ of 1.08 km. Figure 13a plots the values of Λ and d_+ as functions of both U and $\overline{U}$. If, instead, a total of 10^3 m^3 of suspension of volume concentration 5% is instanteously released from a point source the radial scale r_p is 176 m. Figure 13b plots the values of λ and r_+ as functions of U and $\overline{U}$. We see clearly that as the mean velocity increases, advection becomes relatively more important and Λ (or λ) increases while at the same time the maximum upstream penetration distance decreases. Sewage refinement tanks are complicated, three-dimensional confined systems with generally a continuous input of untreated, dirty water. Typically quoted parameters for such systems are concentrations between 300 and 3000 mg l^{-1}, which corresponds to particulate concentrations of 0.03 - 0.3 by weight, settling velocities of 1 m hr^{-1} in flow throughs of 1 m hr^{-1} at one end of a tank 40 m long. Consider, for the sake of calculation, a mid-range concentration of 0.1 by volume (with a corresponding $g_p'=10^{-3}g$) and an instantaneous input of cross-sectional area 5 m^2. The length scale l_∞ = 18.6 m. Setting the throughput velocity U equal to the settling velocity V, we can easily calculate that $\Lambda = 0.076$, from which it follows that d$_+$=7.2. Of more significance, maybe, to this particular situation is l_∞-d_+= 11.4 m, which is the maximum *downstream* length scale of the deposit, satisfyingly shorter than the typical tank length of 40 m. It should be recalled however, that in our model some of the particles never settle; a small fraction are swept far downstream.

Increasing the initial volume of particles by a factor of 3, which also increases $g_p'\phi_0$ by a factor of 3, increases l_∞ by a factor of $3^{2/5}\approx1.55$, i.e. to 29 m. Increasing the cross-sectional area has a relatively larger effect. An increase by a factor of 3 increases l_∞ by a factor of $3^{3/5}\approx1.93$ i.e. to 36 m.

For the third example, the particles are so much heavier than the ambient air that g replaces g_p' wherever it appears in the calculations. Consider a particle of density 0.5 g cm^{-3} and diameter 5μm,

a)

b)
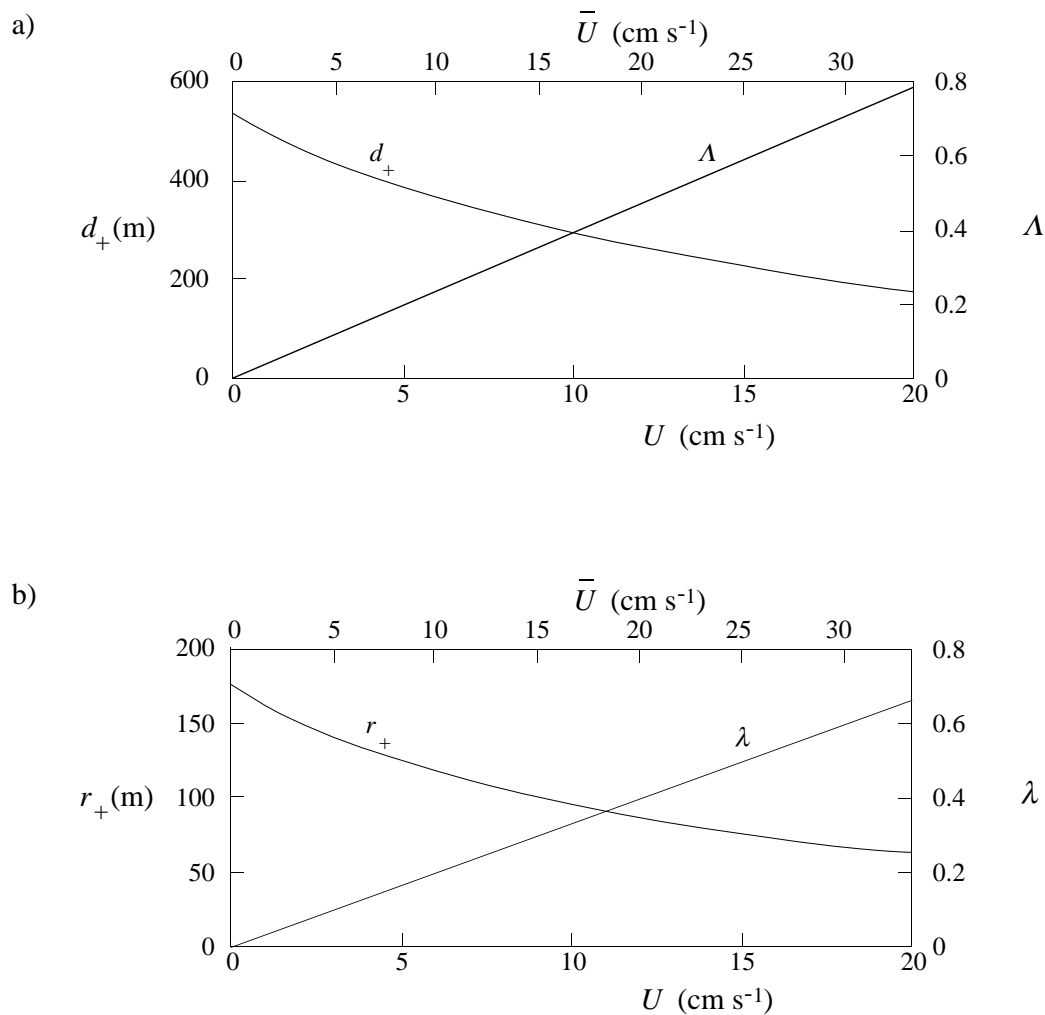
Fig. 13. The maximum upstream penetration distance and the corresponding value of Λ either λ as a function of both the effective velocity U and the mean ambient flow velocity $\overline{U}$ (with $U=0.6\,\overline{U}$) for the instantaneous release of water contaminated with 5% by volume of particles 20 μm in diameter with density 2.0 g cm^{-3}. a) 100 m^2 of contaminated water released into a two-dimensional channel; and b) 1000 m^3 of contaminated water released from a point source into an unconfined system.

which has a settling velocity in air at 20°C of 3.8×10^{-2} cm s^{-1}. A suspension of such particles with volume concentration of 10% and cross-sectional area of 10^5 m^2 corresponds to $l_\infty = 62.9$ km. Figure 14a plots the appropriate values of Λ and d_+ as functions of U and $\overline{U}$. Alternatively, if 1 km^3 is contaminated with a volume concentration of 1% of such particles r_p is 21.9 km. Figure 14b graphs the curves of λ and r_+ as functions of U and $\overline{U}$.

Acknowledgments

References

ALAVIAN, V., JIRKA, G.H., DENTON, R.A., JOHNSON M.C. and STEFAN, H.G.(1992) Density currents entering lakes and reservoirs. *J. Hydr. Engng.* **118**, 1464-1489.

BENJAMIN, T.B. (1968) Gravity currents and related phenomena. *J.Fluid Mech.* **88**, 223--240.

BONNECAZE, R.T., HALLWORTH, M.A., HUPPERT, H.E. and LISTER, J.R. (1995) Axisymmetric particle-driven gravity currents. *J.Fluid Mech.* **294**, 93-121.

BONNECAZE, R.T., HUPPERT, H.E. and LISTER, J.R. (1993) Particle-driven gravity currents. *J.Fluid Mech.* **250**, 339-369.

DADE, W.B. and HUPPERT, H.E. (1994) Predicting the geometry of channelised deep-sea turbidites. *Geology* **22**, 645-648.

DADE, W.B. and HUPPERT, H.E. (1995) Runout and fine-sediment deposits of axisymmetric turbidity currents. *J. Geophys. Res.* **100**, 18,597-18,609.

DE ROOIJ, F. (1999) Sedimenting Particle-laden Currents. Ph.D. Thesis Cambridge University.

HALLWORTH, M.A., HOGG, A.J. and HUPPERT, H.E. (1998) Effects of external flow on compositional and particle gravity currents. *J.Fluid Mech.* **359**, 109-142.

HALLWORTH, M.A., PHILLIPS, J., HUPPERT, H.E. and SPARKS, R.S.J. (1993) Entrainment in turbulent gravity currents. *Nature* **362**, 829-831.
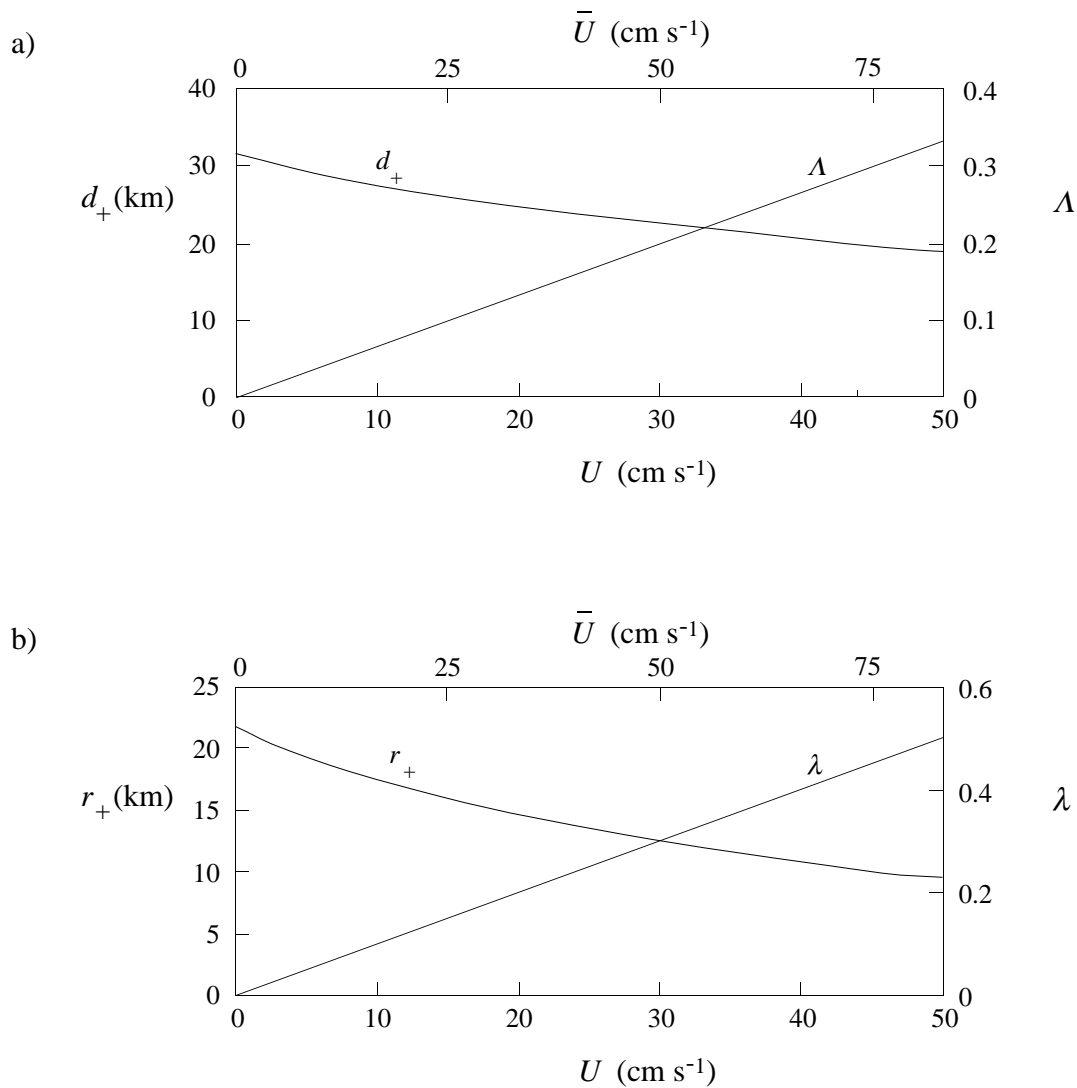
Fig. 14.   The maximum upstream penetration distance and the corresponding value of either Λ or λ as a function of both the effective velocity U or the mean ambient flow velocity $\bar{U}$ (with U=0.6 $\bar{U}$) for the instantaneous release of air contaminated with 10% by volume of particles 5 μm in diameter with density 0.5 g cm^{-3}. a) 0.1 km^2 of contaminated air released into a two-dimensional channel; and b) 1 km^3 of contaminated air released from a point source into an unconfined system.

HALLWORTH, M.A., HUPPERT, H.E., PHILLIPS, J. and SPARKS, R.S.J. (1996) Entrainment into two-dimensional and axisymmetric turbulent gravity currents. *J. Fluid Mech.* **308**, 289-312.

HUPPERT, H.E. (1997) Buoyancy Effects in Fluids *Part III Mathematical Tripos Examination.*

HUPPERT, H.E. (1998) Quantitative modelling of granular suspension flows. *Phil. Trans. Roy. Soc.* **A356**, 2,471-2,496

HUPPERT, H.E and SIMPSON, J.E. (1980) The slumping of gravity currents. *J. Fluid Mech.* **99**, 785-799.

HUPPERT, H.E., KERR, R.C., LISTER, J.R. and TURNER, J.S. (1991) Convection and particle entrainment driven by differential sedimentation. *J.Fluid Mech.* **226**, 349-369.

LANE, S.N, BIRON, P.M., BRADBROOK, K.F., BUTLER, J.B.,

CHANDLER, J.H, CROWELL, M.D., McLELLAND, S.J., RICHARDS, K.S and ROY, A.G. (1998) Three-dimensional measurements of river channel topography and flow processes using acoustic Doppler velocimetry. *Earth Surface Processes & Landforms* **23**, 1247-1267.

MARTIN, D. and NOAKES, R. (1988) Crystal settling in a vigorously convecting magma chamber. *Nature* **332**, 534-536.

SIMPSON, J. E. (1997) Gravity currents in the Environment and the Laboratory. *Cambridge University Press.*

SIMPSON, J. E. and BRITTER, R.E. (1980) A laboratory model of an atmospheric mesofront. *Quart.J.Roy.Met.Soc* **106**, 485-500.

WHITHAM, G.B. (1974) Linear and Nonlinear Waves. *Wiley*, New York.